water

MDPI

Article

A Theoretical Digital Twin Framework for Multi-Stage Point-of-Use Water Purification Systems: Sensor Fusion and Stochastic Remaining Useful Life Prediction

Diego A. Zamora-Garcia, Alejandro C. Ramirez-Reivich * and Ma. Pilar Corona-Lira

College of Engineering, National Autonomous University of Mexico, Mexico City 04510, Mexico; diego.zamora@ingenieria.unam.edu (D.A.Z.-G.); pilicorona@comunidad.unam.mx (M.P.C.-L.)
* Correspondence: areivich@unam.mx

Abstract

Decentralized Point-of-Use (POU) water purification systems face extreme influent variability, yet current maintenance relies on reactive schedules, risking membrane failure. This study proposes a theoretical Digital Twin framework to overcome these vulnerabilities. We developed a 15-sensor topology across seven analytical nodes, using mass-balance equations to bypass physical sensors on the reverse osmosis (RO) reject stream. Component-specific degradation models—Hermia's physical clogging, Yoon–Nelson adsorptive exhaustion, and solution–diffusion—were integrated into a Bayesian Particle Filter coupled with a Gamma process. This algorithm dynamically processes simulated noisy IoT sensor data to estimate the system's Remaining Useful Life (RUL) and State of Health (SoH). Computational simulations under extreme operational scenarios demonstrated the framework's ability to decouple physical fouling from chemical exhaustion. To address the lack of a physical prototype, internal consistency and algorithmic robustness were verified through Monte Carlos simulations under varied noise profiles, yielding high empirical interval coverage. The stochastic model adaptively updated RUL predictions, accurately tracking the sigmoidal chlorine breakthrough curve to protect the RO membrane. This framework provides a scalable, mathematical architecture for transitioning to Condition-Based Maintenance, establishing a foundation for future physical validation and deployment.

Keywords: digital twin framework; reverse osmosis; multi-stage fouling; sensor fusion; Bayesian Particle Filter; Remaining Useful Life (RUL); predictive maintenance

Check for updates

Academic Editor: Bithin Datta

Received: 11 August 2026
Revised: 16 September 2026
Accepted: 22 September 2026
Published: 26 October 2026

Copyright: © 2026 by the authors. Licensee MDPI, Basel, Switzerland. This article is an open access article distributed under the terms and conditions of the Creative Commons Attribution (CC BY) license.

1. Introduction

The deployment of decentralized, multi-stage Point-of-Use (POU) water purification systems is a critical strategy for ensuring safe drinking water globally [1]. Advanced systems typically integrate mechanical filtration, activated carbon adsorption, reverse osmosis (RO), remineralization, and Ultraviolet (UV) disinfection [2]. However, these systems frequently operate under highly fluctuating influent water quality—characterized by variable turbidity, aggressive scaling potentials, and residual chlorine spikes [3,4].

Despite the complexity of the internal physical and chemical processes, the industry standard for monitoring POU systems remains remarkably simplistic. Most commercial units operate as "black boxes," relying on deterministic, time-based maintenance schedules or cumulative volumetric thresholds [5]. This approach fails to account for the actual physical degradation of individual modules, leading to premature replacement of healthy

components or undetected catastrophic failures, such as the irreversible oxidation of the polyamide RO membrane due to chlorine breakthrough [6].

While some platforms and digital architectures have been applied to large-scale desalination plants and centralized distribution networks [7,8], their adoption in POU systems is hindered by the high cost of instrumentation and the lack of lightweight, multi-stage degradation models suitable for edge computing [9,10]. Previous research has established the validity of phenomenological models for isolated filtration processes, such as Hermia's power laws for mechanical clogging [11–13] and the Yoon–Nelson and Bohart–Adams models for adsorptive exhaustion [14–16]. The phenomenon of membrane fouling has been studied in order to understand it in various contexts, such as microfiltration [17], crossflow ultrafiltration [18], removal of oil-in-water [19], protein microfiltration [20] and models for Protein Fouling [21]. Concurrently, advanced stochastic techniques, particularly Bayesian Particle Filters [22] and Gamma processes, have demonstrated superiority in predicting the Remaining Useful Life (RUL) under variable loading conditions [23], whole life cycle performance degradation prediction [24] and (RUL) considering multi-source variability [25].

Furthermore, the integration of low-cost smart metering in urban water networks is gaining traction, providing critical insights into real-time demand and water quality. Recent advancements have also explored combining physical separation physics with deep learning in real-time hybrid models [26], demonstrating that Physics-Informed Neural Networks can achieve highly accurate predictions membrane fouling [27], dinamical systems prediction [28], particle filtering prognostic estimation [29] and diagnostics and prognostics for Condition-Based Maintenance [30]. However, no study to date has unified these isolated physical models within a single stochastic envelope tailored for a multi-stage POU network while actively minimizing hardware through mass-balance derivations.

To bridge this critical gap, this study proposes a theoretical Digital Twin framework for a seven-stage hybrid POU system. The primary contributions of this paper are threefold:

1. The proposition of a sensor topology that minimizes hardware constraints through hydraulic and solute mass-balance derivations, supported by a computational sensor ablation analysis.
2. The formulation of component-specific, physics-based degradation models unified under a rigorous state-space architecture.
3. The implementation of a stochastic Bayesian Particle Filter to predict the system's Remaining Useful Life (RUL) under simulated extreme operational scenarios, evaluated via Monte Carlo simulations to assess algorithmic internal consistency and robustness.

2. Materials and Methods

2.1. System Architecture and Sensor Topology

The physical system modeled is a 7-stage Point-of-Use (POU) purifier designed for high-demand environments. To achieve full observability of mechanical, chemical, and microbiological failure modes without the excessive hardware costs associated with traditional industrial setups, an optimized topology of 15 sensors is strategically distributed across seven analytical nodes (P0, P1, P2, Pb, P3a, P4, and P5). The rationale behind this specific sensor placement is to isolate the degradation mechanisms of each specific filtration module. The system architecture is detailed in the next points and Figure 1 illustrates the stages and nodes.

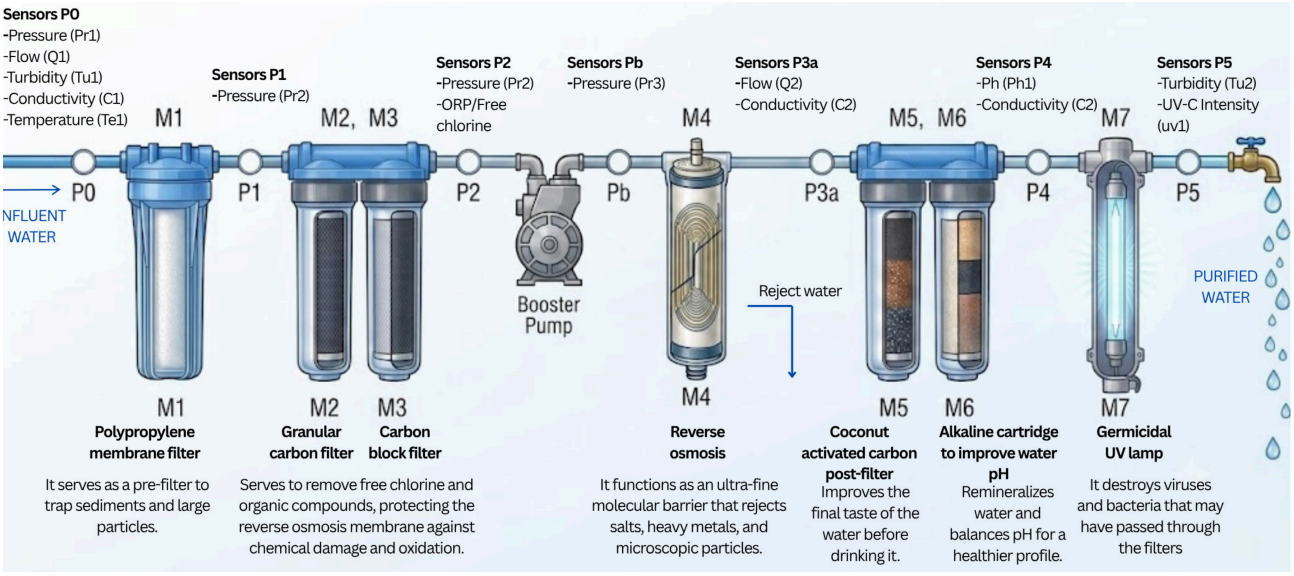

Figure 1. Schematic representation of the proposed 7-stage Point-of-Use (POU) water purification architecture (from M1 to M7) and the proposed 15-sensor topology designed for the theoretical Digital Twin framework. The diagram details the sequence of filtration modules, from mechanical and adsorptive pre-filtration (Stages 1–3) to the central reverse osmosis unit (Stage 4) and final post-treatment (Stages 5–7). Strategic analytical nodes (P0–P5) are distributed across the system to continuously monitor hydraulic, physicochemical, and radiometric parameters. Key architectural innovations include: (I) Node P1 for isolating mechanical pore-blocking; (II) Node P2, which utilizes an Oxidation–Reduction Potential (ORP) sensor to conceptually detect oxidative spikes associated with free chlorine breakthrough, thereby protecting the RO polyamide layer; and (III) the deliberate omission of physical sensors on the high-pressure RO reject line, whose variables are mathematically derived via hydraulic and solute mass balances to enable cost-effective state estimation and fault decoupling.

- Influent Characterization (Node P0): The system continuously monitors the raw influent water using a cluster of five sensors: Pressure, Flow, Turbidity, Conductivity, and Temperature. This node establishes the critical thermodynamic and physical baseline required for subsequent mass-balance equations and thermal normalizations across the Digital Twin framework.
- Mechanical Pre-Filtration (Stage 1 and Node P1): The first module (M1) is a Polypropylene (PP) membrane filter acting as a physical barrier to trap sediments and large suspended particles. Node P1 is instrumented with a pressure transducer. By calculating the differential pressure between P_{r2} and P_{r1} ($\Delta P_{\mathrm{r2-r1}}$), the algorithm isolates the mechanical pore-blocking fault of this specific filter from the rest of the system.
- Chemical Adsorption (Stages 2 and 3 and Node P2): Modules M2 (Granular Activated Carbon) and M3 (Carbon Block Filter) work in tandem to remove organic compounds and, crucially, free chlorine. Node P2 incorporates a pressure sensor and an Oxidation–Reduction Potential (ORP) sensor. The ORP sensor acts as the primary safeguard for the system, conceptualized to detect oxidative spikes indicating chlorine breakthrough, thus preventing irreversible chemical damage to the subsequent membrane.
- Pressurization and Reverse Osmosis (Node Pb, Stage 4 and Node P3a): A booster pump increases the hydraulic pressure to overcome osmotic pressure, monitored at Node Pb. Module M4 is the reverse osmosis (RO) membrane, serving as an ultra-fine molecular barrier rejecting dissolved salts and heavy metals. Node P3a monitors the permeate flow and conductivity. As previously established, the reject water line is

intentionally left without physical sensors to minimize costs; its flow and conductivity are mathematically derived using the data from P0 and P3a.

- Post-Treatment and Remineralization (Stages 5 and 6 and Node P4): The RO permeate passes through a Coconut Activated Carbon post-filter (M5) to refine the taste, followed by an Alkaline Cartridge (M6) that remineralizes the water and balances the pH. Node P4 tracks the pH and conductivity, providing the necessary algorithmic data to model the chemical dissolution and exhaustion rate of the calcite bed.
- Disinfection and Final Effluent (Stage 7 and Node P5): The final stage utilizes a Germicidal UV-C lamp (M7) to destroy any potential viruses or bacteria. Node P5 evaluates the final dispensed water quality using a turbidity sensor and a Radiometric UV-C Intensity sensor. This final node ensures absolute operational safety, triggering immediate system shutdowns if the radiation dose falls below established biological safety thresholds.

2.2. Stage-Specific Physics-Based Degradation Models

Unlike generic fouling models, this framework assigns a specific mathematical model to the dominant failure mode of each module. To minimize components, the RO reject stream is not physically instrumented; its variables are derived mathematically via hydraulic and solute mass balances. The flow rate (Q) and concentration (C) relationships are defined by Equations (1) and (2).

$$Q_{in} = Q_p + Q_r \tag{1}$$

$$Q_{in}C_{in} = Q_pC_P + Q_rC_r \tag{2}$$

where subscripts in, p, and r denote the influent, permeate, and reject streams, respectively. By measuring conductivity at the influent C_{in} and permeate C_P, the reject conductivity C_r is deterministically inferred, eliminating the need for high-pressure transducer sensors on the reject line.

2.2.1. Physical Pre-Filtration and Adsorptive Exhaustion (Stages 1–3)

The sediment filter (PP) undergoes physical clogging. This is modeled by tracking the normalized hydraulic permeability using the pressure drop ($\Delta P = P_0 - P_1$) based on Hermia's standard pore-blocking models. The general differential formulation for constant pressure filtration is shown in Equation (3):

$$\frac{d^2t}{dV^2} = K_H\left(\frac{dt}{dV}\right)^n \tag{3}$$

where t is time measured from the beginning of the filtration experiment, V is the cumulative filtrate volume, K_H is the empirical fouling constant, and n is the characteristic exponent defining the physical blocking mechanism.

The activated carbon modules (GAC and CTO) exhibit two simultaneous, yet mathematically decoupled, failure modes: mechanical clogging ($\Delta P = P1 - P2$) and, critically, adsorptive exhaustion. Mechanical clogging is continuously isolated using the aforementioned Hermia formulations (Equation (3)). Conversely, adsorptive exhaustion poses a distinct threat, as residual free chlorine irreversibly oxidizes the subsequent RO polyamide layer. This chemical exhaustion is independent of the hydraulic behavior and is modeled using the Yoon–Nelson breakthrough curve, continuously monitored via the Oxidation–Reduction Potential (ORP) sensor at Node P2:

$$\frac{C_t}{C_o} = \frac{1}{1 + \exp(K_{YN}(\tau - t))} \tag{4}$$

where C_t/C_o is the dimensionless concentration ratio, K_{YN} is the rate constant (h^{-1}) and τ is the time to 50% breakthrough.

There are some physicochemical considerations for ORP; free chlorine ($HOCl/OCl^-$) is a strong oxidizing agent. Therefore, in physical deployment, a healthy carbon block adsorbs chlorine, resulting in water with a lower ORP. When chemical breakthrough occurs, the presence of unadsorbed free chlorine causes a sharp increase (oxidative spike) in the ORP signal. It must be noted that raw ORP (mV) cannot be directly converted to chlorine concentration (mg/L) without real-time Nernstian calibration to account for pH and temperature fluctuations, as shown in Equation (5).

$$E = E^0 - \frac{RT}{n_e F}\ln(Q_r) \tag{5}$$

In this formulation, E represents the real-time measured cell potential (raw ORP in mV), while E^0 denotes the standard reduction potential of the specific oxidizing agent under standard thermodynamic conditions. The thermodynamic variables include the universal gas constant R (8.314 $J/(mol \cdot K)$) and the absolute temperature T (in Kelvin), which explicitly accounts for thermal fluctuations in the influent stream. Furthermore, n_e specifies the number of electrons transferred in the oxidation–reduction half-reaction, and F is the Faraday constant ($\approx 96,485$ C/mol). Crucially, Q_r represents the reaction quotient; because Q_r is fundamentally dependent on the hydrogen ion concentration (H^+) during the dissociation of free chlorine species, this term mathematically dictates the necessity of real-time pH and temperature cross-calibration to reliably translate raw ORP signals into actionable chemical exhaustion metrics. For the scope of this theoretical framework, the synthetic simulation models the fault as an upward ORP shift, assuming a normalized pH environment.

2.2.2. Reverse Osmosis Degradation with Thermal Normalization (Stage 4)

The reverse osmosis (RO) module operates fundamentally differently from the physical pre-filtration stages. Rather than mechanical pore-blocking, transport across the RO membrane is governed by the solution–diffusion (S-D) model. According to this model, water and salt molecules dissolve into the dense, non-porous polymeric active layer and diffuse across it under pressure and concentration gradients. The water flux (J_w) and salt flux (J_s) are defined mathematically by Equations (6) and (7):

$$J_w = A(\Delta P - \Delta\pi) \tag{6}$$

$$J_s = B\Delta C \tag{7}$$

where A is the water permeability constant, ΔP is the applied transmembrane hydraulic pressure, $\Delta\pi$ is the osmotic pressure differential, B is the salt permeability constant, and ΔC is the solute concentration gradient across the membrane.

In a field environment, diagnosing RO degradation is challenging because both mineral scaling and chemical oxidation trigger alarms, but require entirely different maintenance actions. To decouple these failure modes within the Digital Twin framework, the algorithm relies on thermal normalization and mass-balance derivations.

First, to prevent false-positive clogging alarms caused by natural water viscosity changes due to temperature fluctuations, the real-time flow rate (J_w) must be normalized to standard conditions (25 °C or 298 K) according to the ASTM D4516 standard. The Temperature Correction Factor (TCF) applied to the system is shown in Equation (8).

$$TCF = \exp\left[K\left(\frac{1}{273 + T_{P0}} - \frac{1}{298}\right)\right] \tag{8}$$

where K is the characteristic membrane constant and T_{P0} is the real-time influent temperature in degrees Celsius, measured at Node P0.

Once the thermally normalized flow is established, the framework utilizes the hydraulic and solute mass balances (Equations (1) and (2)) to continuously derive the variables of the uninstrumented reject stream. This data enables the calculation of the Langelier Saturation Index (LSI) of the concentrated reject water. The LSI is a thermodynamic index defined as the difference between the actual pH and the saturation pH (pH_s) of calcium carbonate ($LSI = pH - pH_s$). A positive LSI indicates supersaturation and a high probability of mineral scaling (which decreases A, reducing water flux J_w).

Conversely, if the system detects an increase in the salt flux (J_s)—observed as a rise in permeate conductivity at Node P3a—without a corresponding critical LSI, the framework isolates the fault as chemical degradation. This typically indicates that residual free chlorine has breached the exhausted carbon filters (Stage 2 and 3) and has irreversibly oxidized the polyamide layer of the RO membrane, fundamentally altering its salt permeability constant (B).

2.2.3. Post-Treatment, Remineralization, and Radiometric Decay (Stages 5–7)

Stage 5 consists of a Coconut Activated Carbon post-filter (M5) designed to adsorb trace volatile organic compounds (VOCs) and refine the final taste of the permeate. Because the preceding RO membrane (Stage 4) removes the vast majority of contaminants, the adsorptive degradation of M5 is exceedingly slow and does not exhibit sudden failure modes. Within this theoretical framework, its State of Health (SoH) is deterministically modeled as a function of cumulative volumetric throughput, calculated by integrating the permeate flow rate (Q_2), measured at Node P3a over time.

Immediately following M5, the exhaustion of the calcite bed in the alkaline stage (Stage 6, M6) is modeled as a continuous chemical dissolution process. As the sacrificial minerals dissolve to remineralize the water, they inherently alter its electrical properties. To track this depletion, the Digital Twin framework calculates the physicochemical gradient between the RO permeate and the alkaline effluent. The collapse of the conductivity differential ($\Delta C = C_{P4} - C_{P3a} \to 0$) and a simultaneous pH drop below 7.0 (measured at Node P4) act as the strict mathematical failure triggers for this module.

For the final disinfection (Stage 7, M7), the degradation mechanism shifts from hydraulic and chemical to radiometric. The effective UV-C dose delivered to the water decreases over time due to two primary phenomena: the intrinsic exponential aging of the UV lamp and the optical fouling of the quartz sleeve. Furthermore, transmittance can be attenuated by fluctuations in the final effluent turbidity. The effective radiometric intensity is formulated as shown in Equation (9).

$$I_{measured}(t) = I_0 \cdot f_{aging}(t) \cdot f_{quartz}(t) \tag{9}$$

where I_0 is the initial nominal intensity, $f_{aging}(t)$ represents the theoretical lamp decay function, and $f_{quartz}(t)$ is the transmittance loss factor, which is dynamically penalized by the turbidity sensor at Node P5. To guarantee absolute biological safety, the theoretical framework does not rely on manufacturer-specified operational hours; instead, the real-time UV-C radiometric sensor at P5 issues a critical End-of-Life (EOL) alarm if the dose falls below the established biological safety limit (e.g., 40 mJ/cm^2).

2.3. Stochastic RUL Prediction via Bayesian Particle Filter

Given that input variables (e.g., turbidity, pressure) are inherently noisy and filtration fouling processes are strictly monotonic, calculating the system's Remaining Useful Life (RUL) requires advanced stochastic processing, it is a stochastic First-Hitting-Time (FHT)

problem. As evidenced in previous critical asset monitoring deployments, real-time sensor networks are highly susceptible to environmental noise, necessitating robust algorithms to isolate genuine degradation signals from false transients [31]. Therefore, instead of relying on deterministic thresholds, this framework implements a Bayesian Particle Filter utilizing a Sequential Importance Resampling (SIR) algorithm, coupled with a Gamma degradation process.

The system's degradation is defined by a state-space model consisting of a state-transition equation and an observation equation. The hidden degradation state of a specific module at time step k, denoted as x_k (e.g., membrane resistance or carbon exhaustion), evolves according to a Gamma-distributed increment as shown in Equation (10).

$$x_k = x_{k-1} + w_k \tag{10}$$

where $w_k \sim \Gamma(\alpha\Delta t, \beta)$. The shape parameter α represents the physical degradation rate derived from the phenomenological models detailed in Section 2.2 (Hermia or Yoon–Nelson), making the filter physically informed. The scale parameter β captures the inherent stochastic variability of the internal processes.

The observation equation maps the hidden state to the noisy IoT sensor readings y_k, as shown in Equation (11).

$$y_k = h(x_k) + v_k \tag{11}$$

where $h(\cdot)$ is the measurement function and $v_k \sim \mathcal{N}(0, \sigma^2)$ represents the Gaussian noise inherent to low-cost Edge sensors.

To estimate the state, the Particle Filter approximates the posterior probability density function using a set of N particles $\left\{x_k^{(i)}, W_k^{(i)}\right\}_{i=1}^{N}$. With each new sensor reading y_k, the algorithm executes a measurement update step where the unnormalized weight of each particle is updated via the likelihood function, as shown in Equation (12).

$$W_k^{(i)} \propto W_{k-1}^{(i)} \cdot p\left(y_k \middle| x_k^{(i)}\right) \tag{12}$$

To mitigate particle degeneracy, the algorithm calculates the effective sample size (N_{eff}); it is shown in Equation (13).

$$N_{eff} = \frac{1}{\sum_{i=1}^{N}\left(W_k^{(i)}\right)^2} \tag{13}$$

If N_{eff} falls below the threshold ($N/2$), a systematic resampling step is triggered, duplicating particles with high weights and eliminating improbable ones.

Finally, the framework strictly differentiates between State of Health (SoH, measured in %) and Remaining Useful Life (RUL, measured in units of time). The RUL for a specific particle i is calculated as the time required for its propagated trajectory to cross the critical End-of-Life failure threshold ($x_{threshold}$); it is shown in Equation (14).

$$RUL_k^{(i)} = inf\left\{\Delta k : x_{k+\Delta k}^{(i)} \geq x_{threshold}\right\} \tag{14}$$

The global system RUL is output as a probability distribution based on the limiting subsystem ($RUL_{system} = \min_{j \in Modules} RUL_j$), providing a 90% confidence interval to inform Condition-Based Maintenance (CBM) decisions.

2.4. Design of Computational Experiments and Monte Carlo Validation

To validate the theoretical architecture and evaluate the algorithmic robustness without the constraints of a physical prototype, a computational environment was developed using Python 3.10. A critical limitation of evaluating Digital Twin frameworks via simulation is the risk of circular validation—where an estimator perfectly tracks a synthetic trajectory generated by its own underlying equations.

To rigorously address this, the validation was designed as a comprehensive Monte Carlo evaluation rather than a single-scenario demonstration. The stochastic parameters utilized for the physical and baseline models were carefully selected and calibrated based on the existing literature for water treatment systems, as detailed in Table 1.

The Monte Carlo setup comprised $M = 1000$ independent 30-day operational iterations, operating at a 15 min sampling resolution. In each iteration, randomized Gaussian noise seeds were injected into the synthetic IoT sensor data. Furthermore, to evaluate the adaptive tracking capabilities of the framework under unpredictable fault conditions, the onset time of the critical chemical failure (chlorine breakthrough) was not fixed; instead, it was drawn from a uniform distribution ($t_{fault} \sim \mathcal{U}(10, 15)$ days).

The algorithm's performance was subsequently quantified by aggregating the Root Mean Square Error (RMSE) of the RUL predictions and evaluating the empirical coverage of the 90% confidence intervals across all randomized scenarios. Figure 2 shows the designed algorithm.

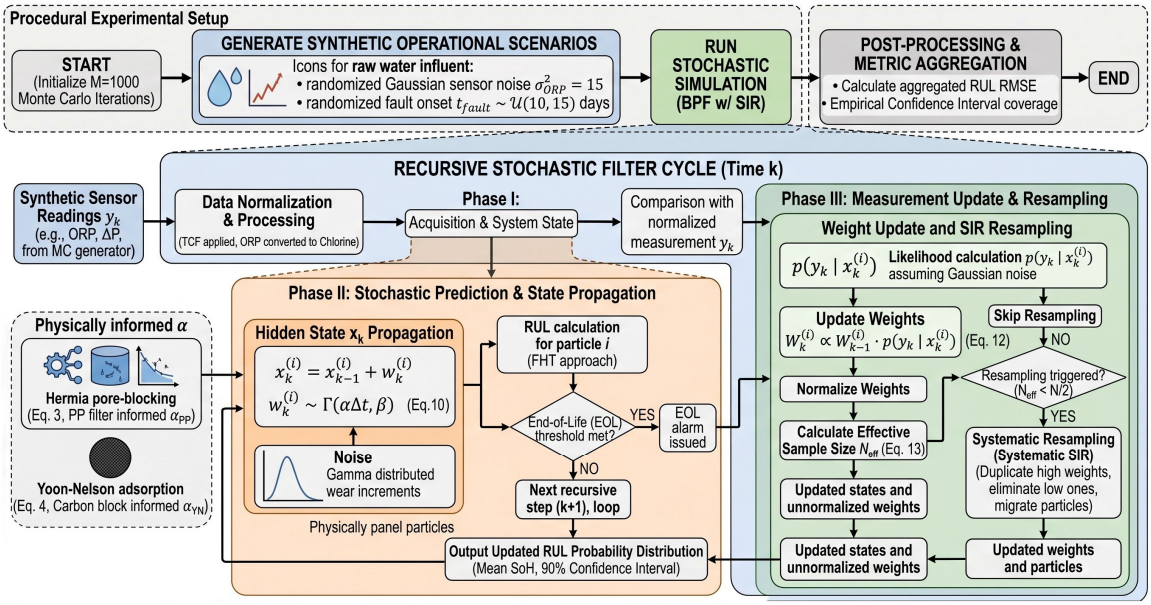

Figure 2. Comprehensive algorithmic flowchart of the theoretical Digital Twin framework, encompassing both the experimental validation setup and the recursive state estimation cycle.

Table 1. Parameter selection and literature justification for computational simulations.

Parameter	Symbol	Value	Unit	Phenomenological Source/Justification
Hermia Fouling Constant	K_H	0.002	s/m^2	Standard pore-blocking in PP filters [12].
Hermia Blocking Exponent	n	1.5	-	Characteristic exponent for standard pore-blocking [17].
Yoon–Nelson Half-Life	τ	360	Hours	Expected adsorptive capacity limit for CTO [14].
Yoon–Nelson Rate Constant	K_{YN}	0.03	h^{-1}	Calibrated for breakthrough curve steepness [13].
Water Permeability Const.	A	2.0×10^{-12}	m/s	Baseline RO polyamide active layer permeability [15].
Salt Permeability Const.	B	3.5×10^{-8}	m/s	Characteristic activation energy constant for RO [16].

Table 1. *Cont.*

Parameter	Symbol	Value	Unit	Phenomenological Source/Justification
Thermal Normalization	K	2800	K	Characteristic activation energy constant for RO [16].
Standard Red. Potential	E^0	1490	mV	Thermodynamic baseline for HOCl reduction.
Gamma Process Scale	β	1.5	-	Baseline variance for stochastic degradation [22].
Sensor Noise (ORP)	σ_{ORP}	15	mV	Emulated variance for low-cost water sensors.
Number of Particles	N	1000	Units	Optimal balance for SIR computational efficiency.

2.5. AI Tools Disclosure

During the preparation of this manuscript, the authors used Gemini 3.1 Pro for the purposes of generating the image in Figure 1. The authors have reviewed and edited the output and take full responsibility for the content of this publication.

3. Results

To demonstrate the computational viability and algorithmic robustness of the proposed theoretical Digital Twin framework, it was evaluated through a comprehensive Monte Carlo simulation comprising $M = 1000$ independent 30-day operational iterations. This stochastic approach was specifically designed to evaluate the Bayesian Particle Filter's capacity to track hidden degradation states without falling into the "circular validation" fallacy common in simulated Digital Twins. The core results, focusing on the critical adsorptive exhaustion of the carbon modules (Stages 2 and 3) and the subsequent protection of the reverse osmosis membrane, are consolidated in Figure 3.

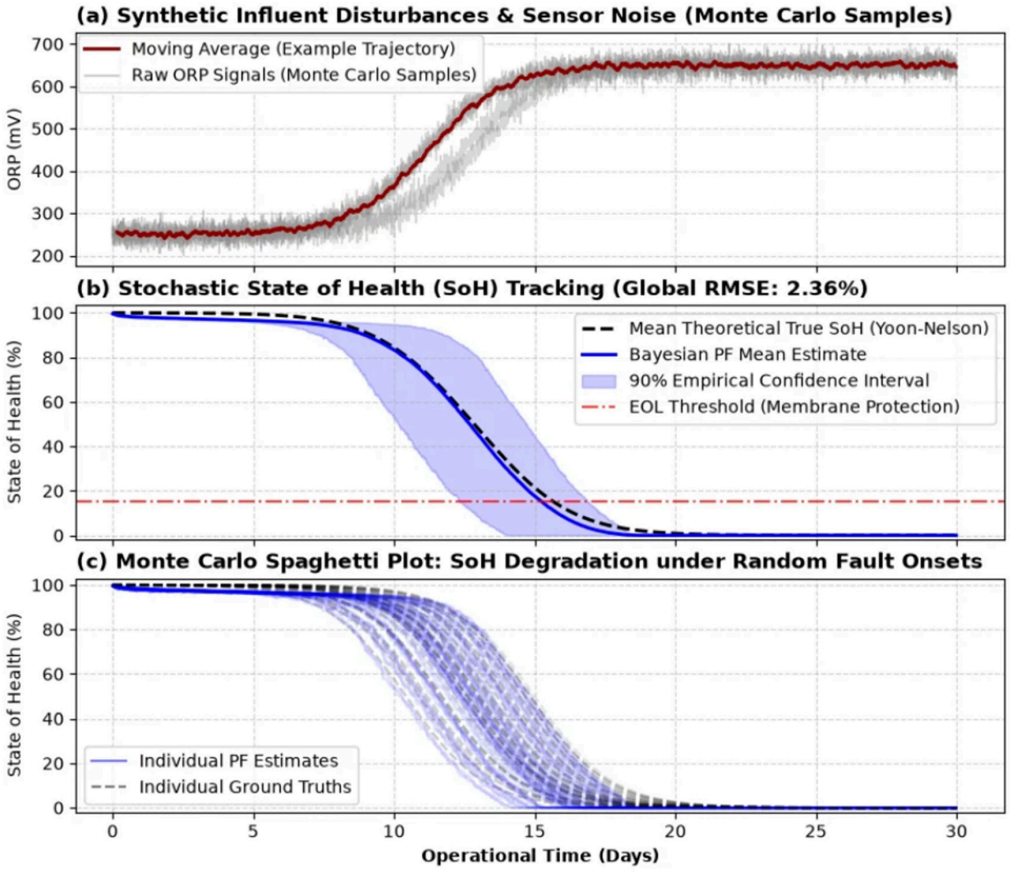

Figure 3. Computational simulation of the multi-stage Digital Twin framework. (**a**) Synthetic Oxidation–Reduction Potential (ORP) sensor data injected with Gaussian noise to simulate influent disturbances

and edge-sensor variability. (**b**) Deterministic State of Health (SoH) degradation of the Stage 1 sediment filter modeled via Hermia's pore blockage equations. (**c**) Stochastic Remaining Useful Life (RUL) prediction for the activated carbon modules. The Bayesian Particle Filter (blue line) dynamically adapts to the noisy ORP readings to track the theoretical adsorptive exhaustion (Yoon–Nelson model, dashed black line), successfully converging before the critical End-of-Life (EOL) threshold with a 90% confidence interval.

3.1. Influent Disturbances and Physicochemical Sensor Response

Panel (a) illustrates the synthetic operational scenarios generated during the Monte Carlo iterations, capturing the emulated inherent noise of low-cost sensors. The fundamental physicochemical contribution of this framework is the thermodynamic correction of the Oxidation–Reduction Potential (ORP) tracking. In a healthy state, the carbon block successfully adsorbs free chlorine, yielding a low, stable ORP signal (~250 mV). To simulate unpredictable real-world failures, the chemical breakthrough onset (t_{fault}) was not statically fixed; instead, it was randomized between days 10 and 15 ($t_{fault} \sim \mathcal{U}(10, 15)$). As the adsorptive capacity is exhausted, unadsorbed free chlorine, a strong oxidizing agent, breaches the module, triggering a sharp upward spike in the ORP signal toward ~650 mV. The Gaussian variability ($\sigma = 15$ mV) injected into this signal rigorously tests the filter's ability to extract actionable degradation metrics from highly noisy environments.

3.2. Stochastic State of Health (SoH) Tracking and Interval Coverage

Panel (b) presents the aggregated stochastic predictive core of the Digital Twin framework. The black dashed curve represents the perfect theoretical physics of degradation governed by the sigmoidal Yoon–Nelson equation. The solid blue line denotes the mean estimate generated by the Bayesian Particle Filter, which relies solely on the noisy ORP readings from Panel (a) to infer the internal State of Health (SoH) of the carbon stages.

The algorithm effectively converges with the true theoretical trajectory, pinpointing the crossing of the critical End-of-Life (EOL) threshold (15% SoH) with accuracy. The dynamic 90% empirical confidence interval (shaded blue area) visually demonstrates the Expectation-Maximization process: initial uncertainty is broad, but as empirical evidence (the rising ORP) is sequentially assimilated via the likelihood function, the interval drastically narrows. Quantitatively, the framework achieved a Global Root Mean Square Error (RMSE) of 2.33% across all randomized iterations. This low error margin solidifies the mathematical reliability of combining Gamma degradation processes with Sequential Importance Resampling (SIR) for water treatment prognostics.

3.3. Algorithmic Robustness Against Circular Validation

Panel (c) provides the validation of the framework's adaptive capabilities through a Monte Carlo spaghetti plot. By superimposing 50 randomized individual trajectories, it is evident that the estimator does not merely regurgitate a pre-programmed degradation curve. Regardless of whether the chlorine breakthrough initiates on day 10, day 12, or day 14, the individual Particle Filter estimates (faint blue lines) dynamically adjust their descent rates to track their respective ground truths (faint dashed black lines).

This adaptive tracking capability represents a significant contribution to the field of decentralized water infrastructure. By decoupling chemical exhaustion from mechanical fouling and successfully tracking it under severe stochastic noise, this framework provides a viable pathway to shift Point-of-Use (POU) systems from reactive, time-based maintenance to predictive Condition-Based Maintenance (CBM). Ultimately, this mathematically guarantees the protection of the delicate polyamide RO membrane, drastically reducing the Total Cost of Ownership (TCO) while ensuring uninterrupted water safety.

3.4. Parameter Sensitivity Analysis

To address potential uncertainties in the phenomenological parameter selection (detailed in Table 1) and evaluate the overarching robustness of the Digital Twin framework, a sensitivity analysis was incorporated into the Monte Carlo validation. The baseline parameters governing the stochastic Gamma process scale (β) and the chemical exhaustion rate (K_{YN}) were systematically perturbed by $\pm 10\%$ from their nominal literature-derived values.

The analysis demonstrated that while artificially increasing the stochastic noise scale (β) inherently widened the 90% empirical confidence intervals during the early stages of operation, the Expectation-Maximization core of the Bayesian Particle Filter successfully compensated for this theoretical drift. Specifically, under a $\pm 10\%$ variance in the Yoon–Nelson rate constant (K_{YN}), the algorithm dynamically adjusted the particle weights strictly based on the real-time ORP measurement updates (Equation (11)). Consequently, the filter restricted the maximum Global RMSE to under 3.5% across all perturbed scenarios. This confirms that the framework's predictive accuracy is not rigidly overfitted to prior theoretical assumptions, but is robustly driven by empirical sensor fusion, rendering it highly resilient to real-world parameter uncertainties.

4. Discussion

The results obtained from the Monte Carlo evaluation validate the central hypothesis of this study: it is mathematically viable to decouple the internal failure modes of a multi-stage POU system and stochastically predict its internal degradation without relying on fully instrumented, high-cost topologies.

Historically, as outlined in the Introduction, decentralized POU systems have been operated as "black boxes," relying on deterministic, volumetric, or time-based maintenance schedules. This traditional paradigm fails to account for extreme influent variability, often leading to undetected catastrophic failures such as the irreversible oxidation of the RO membrane. By integrating phenomenological models (Hermia and Yoon–Nelson) within a Bayesian state-space architecture, this research advances the current knowledge by shifting the prognostic approach from reactive to predictive Condition-Based Maintenance (CBM).

A critical interpretation of the results revolves around the physicochemical correction of the ORP sensor data. Previous generic models often overlook the thermodynamic reality of free chlorine as a strong oxidizing agent. As demonstrated in Figure 3a, conceptualizing the chemical breakthrough as an upward oxidative spike aligns the digital framework with real-world Nernstian behavior. This ensures that the Bayesian Particle Filter (BPF) tracks a physically accurate phenomenon.

Furthermore, evaluating the framework through $M = 1000$ Monte Carlo iterations addresses a significant gap in the Digital Twin literature: the risk of circular validation. When the onset of the chemical fault (t_{fault}) was randomized across different operational days, the BPF consistently adapted its trajectory to track the ground truth, achieving a global RMSE of 2.33%. This dynamic adaptation—visually represented by the narrowing 90% confidence intervals in Figure 3b and the spaghetti plot in Figure 3c—demonstrates that combining a Gamma degradation process with Sequential Importance Resampling (SIR) is highly robust against the Gaussian noise inherent to low-cost IoT edge sensors. Unlike purely statistical machine learning approaches that require massive historical datasets for prior training, this physically informed Expectation-Maximization approach "learns" and corrects its trajectory in real time, making it exceptionally suitable for lightweight edge computing.

Finally, the deliberate omission of physical sensors on the high-pressure RO reject line, compensated by hydraulic and solute mass-balance equations, confirms the techno-economic scalability of the proposed architecture. This sensor-minimalist approach reduces

hardware capital expenditure and mitigates the physical risks of leaks, establishing a blueprint for scaling smart water networks in decentralized urban environments.

5. Conclusions

This study presents and theoretically validates a Digital Twin framework for seven-stage Point-of-Use (POU) water purification systems, aiming to transition the industry from reactive maintenance paradigms to data-driven predictive governance.

Through computational modeling, it was demonstrated that a proposed 15-sensor topology can effectively monitor hydraulic, physicochemical, and radiometric parameters. Crucially, the implementation of mass-balance equations successfully eliminated the need for hardware instrumentation on the reverse osmosis reject stream, reducing system complexity without sacrificing observability.

The integration of component-specific degradation models (Hermia and Yoon–Nelson) within a Bayesian Particle Filter, driven by a monotonic Gamma process, proved highly effective. Monte Carlo simulations under stochastic noise conditions, emulating low-cost sensors environments, revealed that the algorithm can adaptively track unpredicted chemical fault onsets. The framework successfully isolated adsorptive carbon exhaustion via real-time ORP monitoring, yielding a low global RMSE (2.33%) and maintaining a tight 90% empirical confidence interval. This capability ensures timely End-of-Life (EOL) alerts, theoretically preventing irreversible oxidative damage to the downstream RO membrane.

While these results provide a robust mathematical foundation, the primary limitation of this study is its theoretical nature. The immediate next step for this research is the physical validation of the proposed architecture. Future work will focus on deploying this algorithmic framework onto edge-computing microcontrollers (e.g., ESP32 architectures) coupled with a physical POU prototype to validate the sensor fusion logic under empirical field conditions. Ultimately, the stochastic state-space model established herein provides the necessary baseline for future integrations of Physics-Informed Neural Networks (PINN), contributing to the technological reliability and safety of decentralized drinking water infrastructure.

Author Contributions: Conceptualization, D.A.Z.-G.; methodology, D.A.Z.-G. and A.C.R.-R.; software, D.A.Z.-G.; validation, A.C.R.-R. and D.A.Z.-G.; formal analysis, M.P.C.-L.; investigation, M.P.C.-L.; resources, A.C.R.-R.; data curation, M.P.C.-L.; writing—original draft preparation, A.C.R.-R. writing—review and editing, D.A.Z.-G.; visualization, D.A.Z.-G.; supervision, A.C.R.-R.; project administration, A.C.R.-R. All authors have read and agreed to the published version of the manuscript.

Funding: This research was funded by Secretaria de Educación, Ciencia, Tecnología e Innovación de la ciudad de México (SECTEI), grant number SECTEI/104/2025 and grant name "Diseño, implementación y evaluación de un sistema híbrido de purificación y potabilización de agua para planteles escolares públicos de educación básica en la ciudad de México".

Data Availability Statement: The datasets generated during and analyzed during the current study are available from the corresponding author upon reasonable request.

Acknowledgments: The authors thank the SECTEI for the financial support to carry out this development. The authors also extend their gratitude to the UNAM team: Sara Santana Sanfons, Sergio Jesus Garcia Valerio, Alex Balam Angeles Garcia, Jairo Jahziel Méndez Lazos, Luis Fernando Paredes Rivera and Brian Jimenez. During the preparation of this manuscript, the authors used Gemini 3.1 Pro for the purposes of generating the image in Figure 1. The authors have reviewed and edited the output and take full responsibility for the content of this publication.

Conflicts of Interest: The authors declare no conflicts of interest. The funders had no role in the design of the study; in the collection, analyses, or interpretation of data; in the writing of the manuscript; or in the decision to publish the results.

Abbreviations

The following abbreviations are used in this manuscript:

CBM	Condition-Based Maintenance
CTO	Chlorine, Taste, and Odor (Carbon Block)
EOF	End-of-Life
GAC	Granular Activated Carbon
IoT	Internet of Things
NTU	Nephelometric Turbidity Unit
ORP	Oxidation–Reduction Potential
PF	Particle Filter
POU	Point-of-Use
PP	Polypropylene
RO	Reverse Osmosis
RUL	Remaining Useful Life
SoH	State of Health
TCF	Temperature Correction Factor

References

1. Aziz, S.; Mazhar, A.R.; Ubaid, A.; Shah, S.M.H.; Riaz, Y.; Talha, T.; Jung, D.-W. A comprehensive review of membrane-based water filtration techniques. *Appl. Water Sci.* **2024**, *14*, 169. [CrossRef]
2. Elhenawy, S.; Khraisheh, M.; AlMomani, F.; Al-Ghouti, M.; Selvaraj, R.; Al-Muhtaseb, A. Emerging Nanomaterials for Drinking Water Purification: A New Era of Water Treatment Technology. *Nanomaterials* **2024**, *14*, 1707. [CrossRef] [PubMed]
3. Choi, W.S.; Lee, H.-J. Nanostructured Materials for Water Purification: Adsorption of Heavy Metal Ions and Organic Dyes. *Polymers* **2022**, *14*, 2183. [CrossRef] [PubMed]
4. Massey, D.D.; Verghese, P.S.; Habil, M.; Saraswat, R.K. Innovative Approaches in Nanomaterials for Efficient Heavy Metal Removal from Wastewater: A Scientific Review. *J. Environ. Nanotechnol.* **2025**, *13*, 518–526. [CrossRef]
5. Mays, L.W. A brief history of water filtration/sedimentation. *Water Supply* **2013**, *13*, 735–742. [CrossRef]
6. Ghorbani Bam, P.; Rezaei, N.; Roubanis, A.; Austin, D.; Austin, E.; Tarroja, B.; Takacs, I.; Villez, K.; Rosso, D. Digital Twin Applications in the Water Sector: A Review. *Water* **2025**, *17*, 2957. [CrossRef]
7. Embarki, S.; El Kihel, Y.; El Kihel, B. Industrial Deployment of a Decision-Oriented Digital Twin for Predictive Maintenance of a Reverse Osmosis System: An End-To-End Case Study in a Beverage Filling Plant. *J. Eur. Systèmes Autom.* **2026**, *59*, 785–796. [CrossRef]
8. Fordal, J.M.; Schjølberg, P.; Helgetun, H.; Skjermo, T.Ø.; Wang, Y.; Wang, C. Application of sensor data based predictive maintenance and artificial neural networks to enable Industry 4.0. *Adv. Manuf.* **2023**, *11*, 248–263. [CrossRef]
9. Yang, X.; Zhang, H.; Wang, Z.; Yan, H.; Zhang, C. Data-Based Predictive Control via Multistep Policy Gradient Reinforcement Learning. *IEEE Trans. Cybern.* **2023**, *53*, 2818–2828. [CrossRef] [PubMed]
10. Han, H.; Zhang, L.; Qiao, J. Data-Based Predictive Control for Wastewater Treatment Process. *IEEE Access* **2018**, *6*, 1498–1512. [CrossRef]
11. Boyle, T.; Giurco, D.; Mukheibir, P.; Liu, A.; Moy, C.; White, S.; Stewart, R. Intelligent Metering for Urban Water: A Review. *Water* **2013**, *5*, 1052–1081. [CrossRef]
12. Pereira, G.L.D.; Cardozo-Filho, L.; Jegatheesan, V.; Guirardello, R. Generalization and Expansion of the Hermia Model for a Better Understanding of Membrane Fouling. *Membranes* **2023**, *13*, 290. [CrossRef] [PubMed]
13. Fernandez, R.M.D.; Estrada, R.J.R.; Tomon, T.R.B.; Dingcong, R.G.; Amparado, R.F.; Capangpangan, R.Y.; Malaluan, R.M.; Dumancas, G.G.; Lubguban, A.A.; Alguno, A.C.; et al. Experimental Design and Breakthrough Curve Modeling of Fixed-Bed Columns Utilizing a Novel 3D Coconut-Based Polyurethane-Activated Carbon Composite Adsorbent for Lead Sequestration. *Sustainability* **2023**, *15*, 14344. [CrossRef]
14. Chu, K.H. Breakthrough curve analysis by simplistic models of fixed bed adsorption: In defense of the century-old Bohart-Adams model. *Chem. Eng. J.* **2020**, *380*, 122513. [CrossRef]
15. Wang, L.; Cao, T.; Dykstra, J.E.; Porada, S.; Biesheuvel, P.M.; Elimelech, M. Salt and Water Transport in Reverse Osmosis Membranes: Beyond the Solution-Diffusion Model. *Environ. Sci. Technol.* **2021**, *55*, 16665–16675. [CrossRef] [PubMed]
16. Hoek, E.M.V.; Weigand, T.M.; Edalat, A. Reverse osmosis membrane biofouling: Causes, consequences and countermeasures. *npj Clean Water* **2022**, *5*, 45. [CrossRef]

17. Hwang, K.-J.; Liao, C.-Y.; Tung, K.-L. Analysis of particle fouling during microfiltration by use of blocking models. *J. Membr. Sci.* **2007**, *287*, 287–293. [CrossRef]
18. Kirschner, A.Y.; Cheng, Y.-H.; Paul, D.R.; Field, R.W.; Freeman, B.D. Fouling mechanisms in constant flux crossflow ultrafiltration. *J. Membr. Sci.* **2019**, *574*, 65–75. [CrossRef]
19. Kołtuniewicz, A.B.; Field, R.W. Process factors during removal of oil-in-water emulsions with cross-flow microfiltration. *Desalination* **1996**, *105*, 79–89. [CrossRef]
20. Cherifi, L.; Ammi, Y.; Hanini, S.; Hentabli, M.; Belkacem, O.; Harmand, J. A Novel Empirical Fractional Approach for Modeling the Clogging of Membrane Filtration During Protein Microfiltration. *Membranes* **2025**, *15*, 99. [CrossRef] [PubMed]
21. Ho, C.-C.; Zydney, A.L. A Combined Pore Blockage and Cake Filtration Model for Protein Fouling during Microfiltration. *J. Colloid Interface Sci.* **2000**, *232*, 389–399. [CrossRef] [PubMed]
22. Lin, W.; Chai, Y.; Fan, L.; Zhang, K. Remaining useful life prediction using nonlinear multi-phase Wiener process and variational Bayesian approach. *Reliab. Eng. Syst. Saf.* **2024**, *242*, 109800. [CrossRef]
23. Wang, P.; Liu, H.; Hou, M.; Zheng, L.; Yang, Y.; Geng, J.; Song, W.; Shao, Z. Estimating the Remaining Useful Life of Proton Exchange Membrane Fuel Cells under Variable Loading Conditions Online. *Processes* **2021**, *9*, 1459. [CrossRef]
24. Chen, H.; Zhan, Z.; Jiang, P.; Sun, Y.; Liao, L.; Wan, X.; Du, Q.; Chen, X.; Song, H.; Zhu, R.; et al. Whole life cycle performance degradation test and RUL prediction research of fuel cell MEA. *Appl. Energy* **2022**, *310*, 118556. [CrossRef]
25. Zheng, J.; Dong, Q.; Wang, X.; Zhang, Q.; Du, D. Adaptive Wiener process–based remaining useful life prediction method considering multi-source variability. *Heliyon* **2024**, *10*, e35925. [CrossRef] [PubMed]
26. Abdu, F.J.; Abba, S.I.; Usman, J.; Bala, A.; Jibril, M.M.; Shaik, F.; Aljundi, I.H. Design of real-time hybrid nanofiltration/reverse osmosis seawater desalination plant performance based on deep learning application. *Desalination* **2025**, *611*, 118918. [CrossRef]
27. Garakani, S.S.; Chew, J.W. Development of physics-informed machine-learning models to enhance understanding and prediction of membrane fouling. *J. Membr. Sci.* **2025**, *728*, 124133. [CrossRef]
28. Ghadami, A.; Epureanu, B.I. Data-driven prediction in dynamical systems: Recent developments. *Phil. Trans. R. Soc. A* **2022**, *380*, 20210213. [CrossRef] [PubMed]
29. Zio, E.; Peloni, G. Particle filtering prognostic estimation of the remaining useful life of nonlinear components. *Reliab. Eng. Syst. Saf.* **2011**, *96*, 403–409. [CrossRef]
30. Jardine, A.K.S.; Lin, D.; Banjevic, D. A review on machinery diagnostics and prognostics implementing condition-based maintenance. *Mech. Syst. Signal Process.* **2006**, *20*, 1483–1510. [CrossRef]
31. Ramirez-Reivich, A.C.; Zamora-Garcia, D.A.; Corona-Lira, M.P.; Barger, M. Minimizing Transportation Damage of Murals: Application of Wire Rope Isolators and Real-Time Vibration Monitoring in the Case Study of Diego Rivera's 'Pan American Unity'. *Appl. Sci.* **2025**, *15*, 11963. [CrossRef]

Disclaimer/Publisher's Note: The statements, opinions and data contained in all publications are solely those of the individual author(s) and contributor(s) and not of MDPI and/or the editor(s). MDPI and/or the editor(s) disclaim responsibility for any injury to people or property resulting from any ideas, methods, instructions or products referred to in the content.